Available online at www.sciencedirect.com
SCIENCE DIRECT®
Journal of Molecular Catalysis A: Chemical 228 (2005) 177–182
JOURNAL OF MOLECULAR CATALYSIS A: CHEMICAL
www.elsevier.com/locate/molcata

X-ray multiple diffraction on the shallow junction of B in Si(0 0 1)

R.V. Orloski[a,*], M.A.A. Pudenzi[a,b,c], M.A. Hayashi[b], J.W. Swart[b,c], L.P. Cardoso[a]

[a] *IFGW, UNICAMP, C.P. 6061, 13083-970 Campinas, SP, Brazil*
[b] *CCS, UNICAMP, C.P. 6061, 13083-970 Campinas, SP, Brazil*
[c] *FEEC, UNICAMP, C.P. 6101, 13083-970 Campinas, SP, Brazil*

Available online 24 November 2004

Abstract

We apply X-ray multiple diffraction (XRMD) as a high resolution probe for analyzing the amorphous-crystalline interface (Si interstitial rich region) for different implantation energies and thermal treatment conditions during the formation of a shallow junction of B implanted in Si(0 0 1) crystals. Renninger scans (RS) (ϕ-scans) of the three sets of samples were measured using the (0 0 2) primary reflection, forbidden by the Si space group. Si(0 0 2) RS of as-implanted samples showed an extra peak coming from the Si interstitial atoms in the implanted region. This hybrid peak provides a very sensitive probe for analyzing the occurrence of interstitial Si atoms close to the amorphous-crystalline interface. We report its behavior as a function of the thermal treatment. The separation between the vacancy rich and the interstitial rich regions explains these results on the basis of the Si interstitial annihilation for shallow implantation. Samples with deep implantation are outside the detection range of the technique, in agreement with results for etched samples.

Keywords: X-ray diffraction; X-ray multiple diffraction; Semiconductors; Ion implantation; Shallow junction

1. Introduction

X-ray diffraction techniques (such as X-ray multiple diffraction (XRMD)) are used to provide structural characterization of materials since they represent a special high resolution probe for analyzing defects in the crystal lattice. XRMD can provide 3D lattice information when different beam orientations within the crystal are simultaneously analyzed. It has enough sensitivity to detect subtle lattice distortions via symmetry changes and can study surface crystalline perfection through surface propagation. Multiple diffraction has been successfully applied as a fine probe to study interfaces in semiconductor epitaxial structures. For example, it provides the characterization of misfit dislocations at the layer/substrate interface plane [1] and of lattice coherence, with the detection of very small changes ($\ll$0.1 Å) in the interface distance [2]. It has also been applied in the study of piezoelectricity in organic crystals [3,4] and recently [5], in the growth modification of KDP crystals by trivalent manganese ions. XRMD is, therefore, a versatile fine microprobe tool for the characterization of interfaces and single crystal surfaces with respect to subtle changes in the crystallographic perfection. Among the possible applications are the study of single crystal model catalysts, such as, metal oxides and metal carbides.

Multiple diffraction arises when an incident beam ($\mathbf{K_0}$) simultaneously satisfies the Bragg law for more than one set of lattice planes within a crystal as shown in Fig. 1. A set of planes called primary ($h_p\ k_p\ \ell_p$), usually parallel to the sample surface, is aligned to diffract the incident beam. The sample is then rotated (ϕ-axis) around the primary reciprocal lattice vector ($\mathbf{H_{01}}$) until several secondary planes ($\mathbf{H_{02}}$) with Miller indices ($h_s\ k_s\ \ell_s$) and arbitrary orientation also diffract. The coupling reflection ($\mathbf{H_{21}}$) is responsible for establishing the intensity interaction between the primary and the secondary reflections (h_p–$h_s\ k_p$–$k_s\ \ell_p$–ℓ_s). The pattern of the primary intensity versus ϕ is called a Renninger scan (RS) [6] and it shows peaks distributed around symmetry mirrors [7] related to the primary vector symmetry and to the ϕ rotation (entrance and exit of a reciprocal lattice point from the Ewald sphere). Special cases of RS under conditions

* Corresponding author. Fax: +55 19 3788 5376.
E-mail address: renata@ifi.unicamp.br (R.V. Orloski).

1381-1169/$ – see front matter © 2004 Elsevier B.V. All rights reserved.
doi:10.1016/j.molcata.2004.09.074

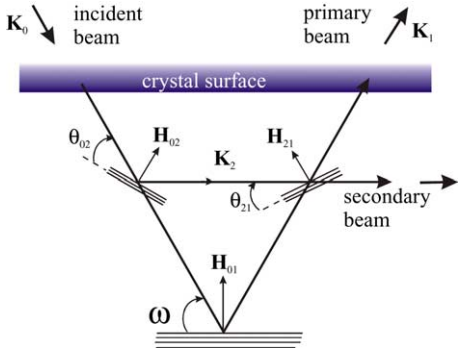

Fig. 1. Planar representation of a BSD case, where $\mathbf{H_{01}}$, $\mathbf{H_{02}}$ and $\mathbf{H_{21}}(=\mathbf{H_{02}}-\mathbf{H_{01}})$ are the primary, secondary and coupling normal vectors, respectively. The coupling planes is responsible to rescatter the secondary beam towards the primary direction.

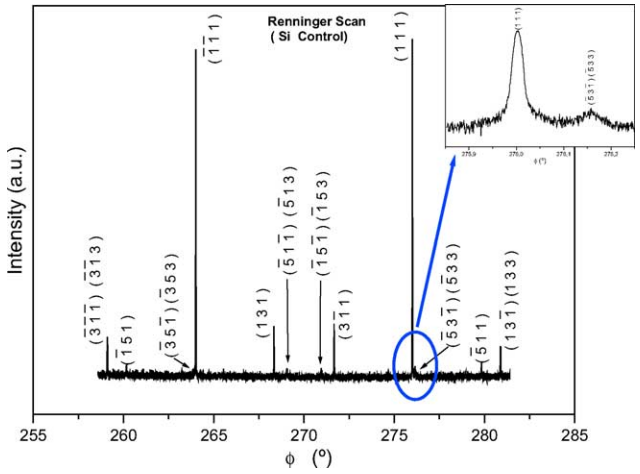

Fig. 3. (0 0 2) Si control indexed RS. Inset shows (1 1 1) BSD peak.

of extreme asymmetry (Bragg surface diffraction (BSD) [8]) appear when the secondary beam is propagated parallel to the sample surface and are very useful for studying crystallographic perfection at the surface or interface. It is also very important to point out that, in semiconductor epitaxial structures, contributions from the layer (substrate) lattice can be obtained in the substrate (layer) RS as extra hybrid peaks [9]. In the case of ion-implanted semiconductors, the occurrence of an implanted region with interstitials within the matrix crystal can be roughly thought of as a layer/substrate system.

The effects of surface finishing processes in semiconductors have been investigated by mapping of the BSD (MBSD) [10] peaks. The regime of diffraction (dynamical, kinematical or mixed) can be directly observed from these mappings by using their 2D projections obtained through the analysis of the ω:ϕ coupled scans [8]. If the crystal is imperfect with small perfect diffracting regions (mosaic blocks), inter-block diffraction takes place and the kinematical diffraction dominates. On the other hand, when the perfect regions become

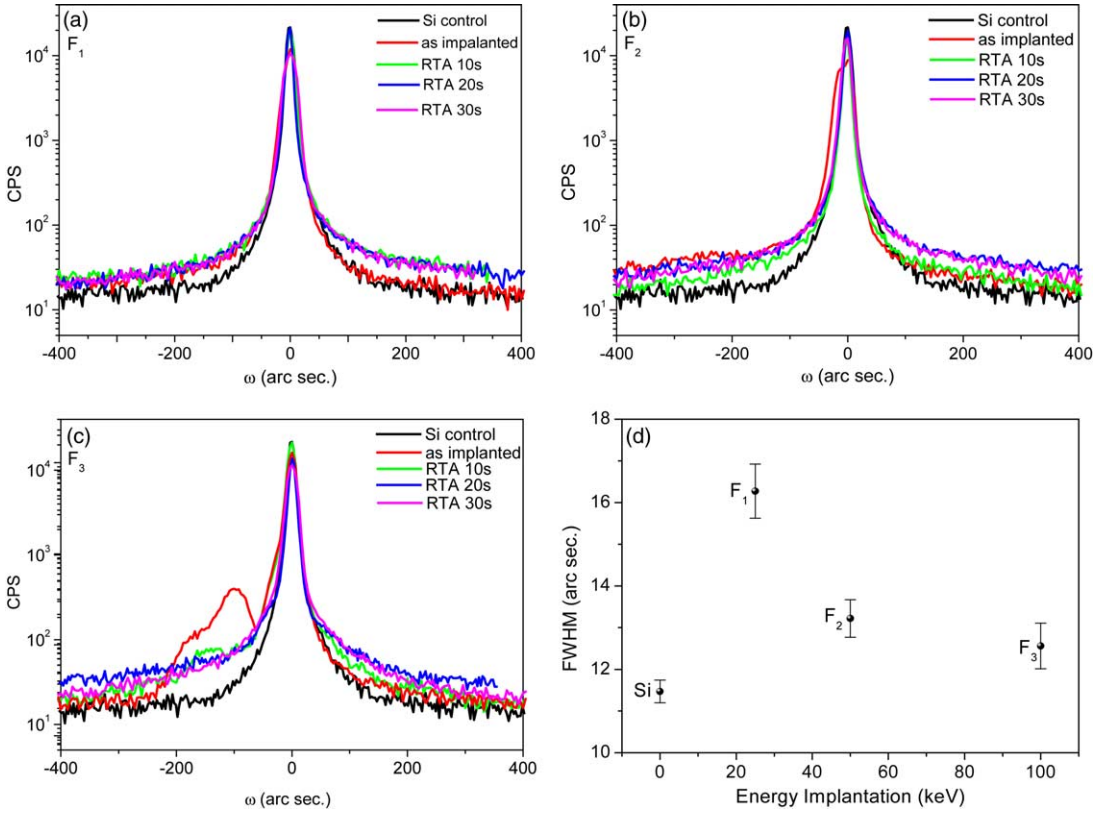

Fig. 2. Rocking curves of Si(0 0 4) for samples: (a) F_1, (b) F_2 and (c) F_3. (d) Plot of the FWHM as a function of the implantation energy for as-implanted Si lattice.

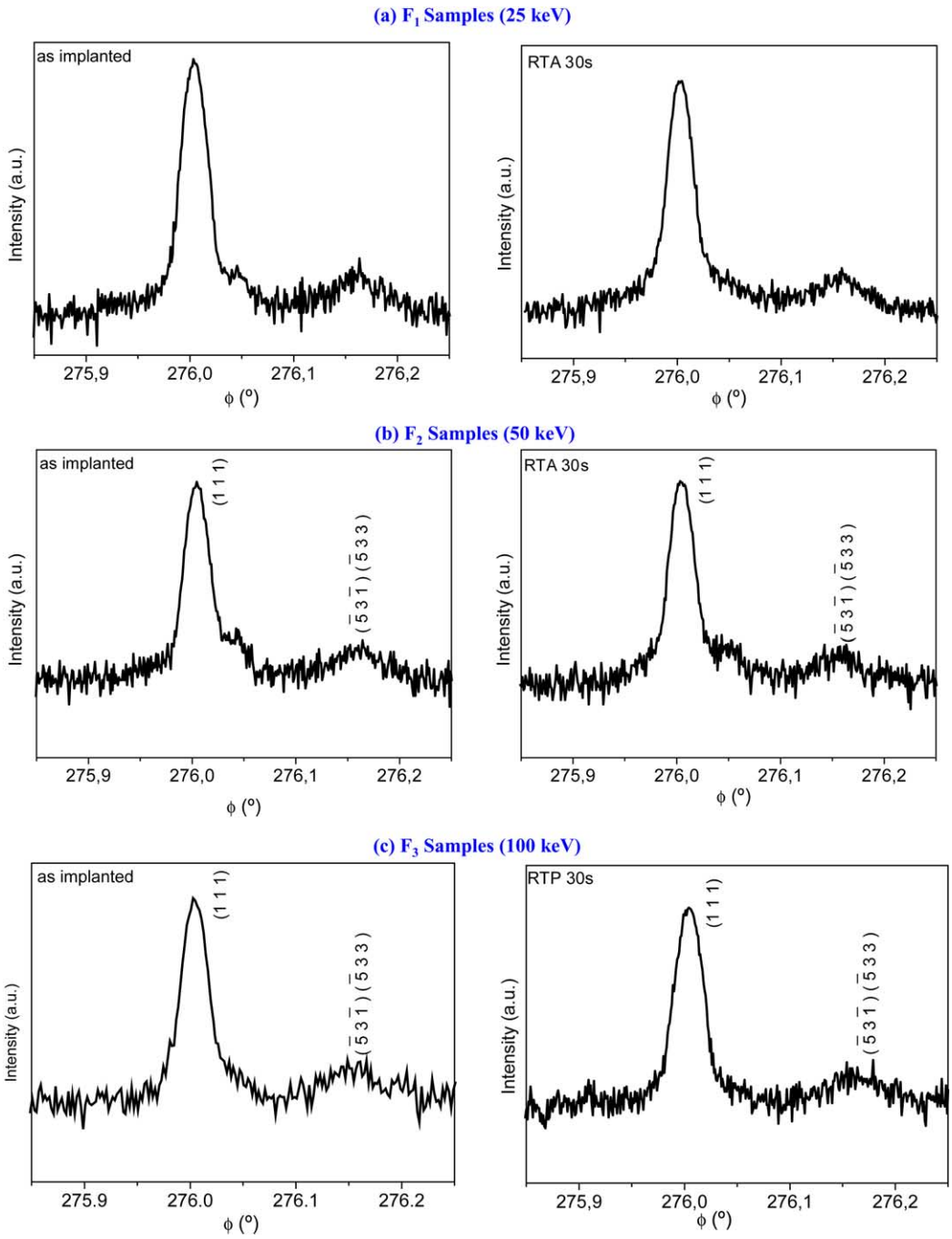

Fig. 4. (1 1 1) BSD peaks for as-implanted and after RTA 30 s samples: (a) F_1, (b) F_2 and (c) F_3.

large enough to allow for intra-block diffraction, the use of dynamical diffraction becomes important. Under this condition, the perfect block dimension affects the peak profile. For semiconductors (even those ion-implanted) intra-block diffraction is usually dominant.

The first successful XRMD application to ion-implanted semiconductors [11] demonstrated its sensitivity to discriminate between the scattering from mosaic and almost perfect crystals and also to study strain in two directions: parallel and perpendicular to the crystal surface. This information are complementary to those obtained by X-ray rocking curves, such as strain distribution profiles in the B implanted Si(0 0 1) wafer before and after laser annealing [12]. In the present work, we discuss the application of the multiple diffraction technique to the study of the conditions for formation of shallow junctions of B in Si(0 0 1). In other words, the extremely

asymmetric BSD cases of the multiple diffraction are used to characterize the amorphous-crystalline interface (interstitial rich region) for different implantation energy and thermal treatment conditions.

2. Experimental

Three sets of Si(0 0 1) wafers were prepared for the experiments. All three were implanted with F^+ of constant dose (2×10^{15} ions/cm^2) with three different implantation energies (25, 50 and 100 keV for samples F_1, F_2 and F_3, respectively) in order to preamorphize the samples. Later, shallow B implantation at 10 keV and 5×10^{14} ions/cm^2 was performed. Each of these three samples suffered rapid thermal annealing (RTA) at 960 °C for 10, 20 and 30 s.

Rocking curves using Cu Kα1 radiation were carried out in a double crystal system under a (±) geometry, which uses a divergent beam generator (50 μm × 50 μm) and is based on a Lang topographic camera with a small Eulerian cradle adapted for sample alignment. We used the (0 0 4) symmetric reflection of a very good GaAs crystal as monochromator.

RS were carried out in a geometry based on a single crystal diffractometer specially developed for this purpose. The incident beam divergences are $\delta_v = 107$ arc seconds and $\delta_h = 149$ arc seconds in the vertical and horizontal planes, respectively. The Cu Kα1 radiation was used in the RS, which were performed with 0.001 degree steps in ϕ-axis. The (0 0 2) reflection forbidden by the Si space group was chosen as primary for the RS in order to provide only secondary peaks in the measured scans. The MBSD measurements (ω:ϕ coupled scans) were carried out at the XDR1 station of the Brazilian National Synchrotron Laboratory (LNLS), Campinas, SP, Brazil, using $\lambda = 1.49765$ Å (using BSD for determination). The geometry consists of two-channel cut Si(1 1 1) crystals as monochromator and a Huber three-axis (ω, ϕ and 2θ) diffractometer fixed on a table, which also provides rotation (χ-axis) around the primary beam direction from 0° to 90°, which allows polarization measurements [13]. The mappings were performed using step sizes of 0.0012° in both, ω- and ϕ-axis.

3. Results and discussion

(0 0 4) Rocking curves of the Si matrix were performed for the F_1 (25 keV), F_2 (50 keV) and F_3 (100 keV) samples. Fig. 2(a) shows the results obtained for the F_1 samples in comparison with the Si control wafer. One can observe that the as-implanted sample presents a small intensity asymmetry at the left side of the peak tail. It indicates a tensile strain (cell expansion) [14] in the crystal lattice due to the excess of interstitial and vacancy point defects. The annealed samples show a symmetric increase of the peak basis intensity, since the first annealing stage (10 s) is sufficient to promote the lattice ion activation.

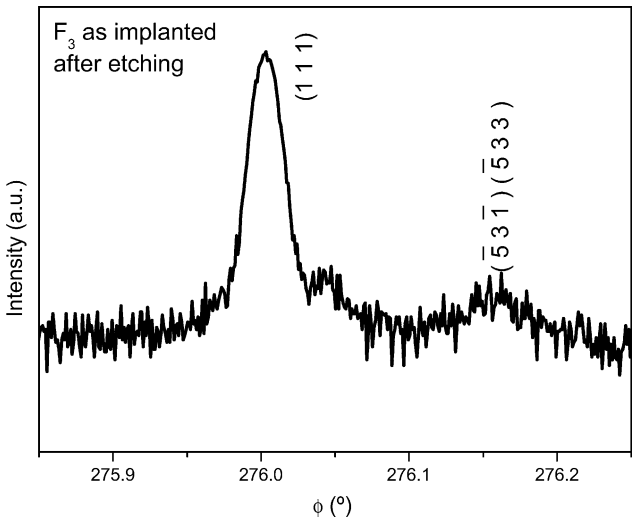

Fig. 5. Effect of the chemical etching in the as-implanted F_3 sample. The hybrid (1 1 1) BSD peak of the RS becomes more defined.

Rocking curves of the F_2 samples together with the control sample appear in Fig. 2(b) and it is observed the initial formation of the implanted region at the left side of the Si(0 0 4) peak (tensile strain) in the as-implanted sample. In this case, the annealing time of 10 s was not enough to promote recrystallization, which was reached only at 20 s.

The results for the F_3 samples are shown in Fig. 2(c) and exhibit fringes also at the left side of the Si peak due to the higher diffracting volume of these samples. One can see that only the 30 s annealing process was sufficient to recrystallize the Si lattice, since a small peak is still observed for the 10 s annealed sample.

The FWHM of the Si(0 0 4) peak plotted as a function of the implantation energy is shown in Fig. 2(d). Narrower peaks are observed for higher implantation energy in the comparison between the as-implanted and Si control samples. The implanted region formation that occurs in higher energy

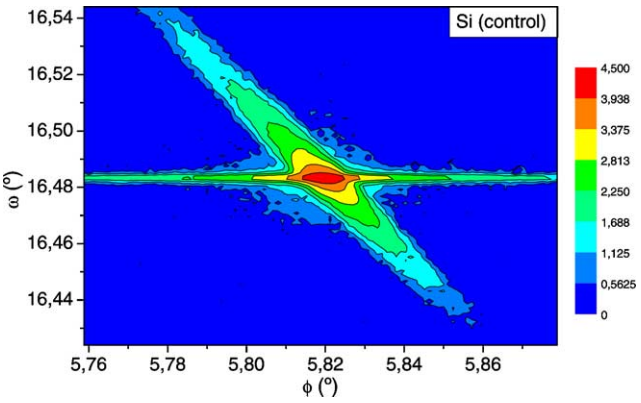

Fig. 6. Mapping of the (1 1 1) BSD of a very good crystallographic Si sample ($W\omega \ll W\phi$) for comparison purposes.

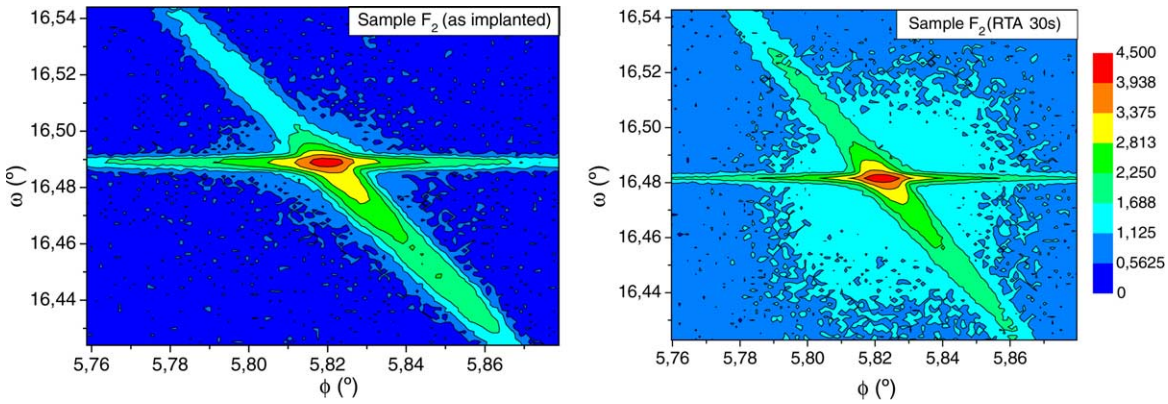

Fig. 7. Mapping of the (1 1 1) BSD F_2 as-implanted samples before and after RTA.

samples causes a matrix cell relaxation, a result also obtained in the analysis of Se doped GaAs (0 0 1) [11].

Fig. 3 shows the (0 0 2) RS around the $\phi = 270^\circ$ symmetry mirror of the Si wafer. The scan is indexed and shows the (1 1 1) strongest BSD peaks that must be analyzed in the case of B shallow junctions in Si. The inset shows the two expected Si peaks: (1 1 1) BSD and $(\bar{5}\,3\,1)(\bar{5}\,3\,3)$ four-beam case. The same angular interval shown in the inset was measured and is presented in Fig. 4 for comparison purposes. The results for the as-implanted and the 30 s RTA for the F_1, F_2 and F_3 samples are depicted in this figure. A weak extra peak observed on the right side of the BSD represents the (1 1 1) BSD implanted region contribution to the matrix RS. In fact, this hybrid [11] contribution comes from the interstitial Si atoms close to the amorphous-crystalline interface (interstitial rich region). In the analysis of the implantation process, the measured hybrids allow the characterization of the implanted region and Si matrix lattices at the same time. Although all the as-implanted scans show this hybrid peak, it is much more pronounced in F_2. After annealing (RTA 30 s) only F_2 samples exhibit the hybrid peak since this thermal energy condition is not enough to activate the lattice ions. The detailed analysis of the implantation conditions and thermal treatment of the F_2 samples will be the subject of a forthcoming paper. The measurements of the other F_1 and F_3 annealed samples (not shown here) also confirm the above-mentioned observation. It is well known that the separation between the vacancies and interstitials increases with the implantation energy due to the momentum transferred to the lattice atoms. Therefore, the Si interstitials concentrate close to the amorphous-crystalline interface whereas the surface becomes a vacancy rich region. This separation is crucial to the hybrid peak detection. For lower implantation energy (F_1 samples), because of the proximity between the vacancy and interstitial regions, thermal annealing promotes their recombination and consequently the disappearance of the hybrid peak. For higher implantation energy (F_3 samples) the recombination is not favored due to the larger separation between these regions and the interstitials survive longer. Nevertheless, the contribution of the interstitials in the as-implanted F_3 sample was barely detected in the matrix RS which indicates the limitation of the BSD probe detection. After chemical etching (HF buffer) to remove 100 nm of the sample, the RS of the F_3 (100 keV) as-implanted sample in Fig. 5 displays a defined hybrid peak, confirming our hypothesis.

The mapping of BSD reflections (MBSD) is very useful for visualizing the distribution of strain in the sample and also to determine whether the analyzed crystal is mosaic (scattering between perfect regions) or dynamical (scattering within perfect regions). Fig. 6 shows the (1 1 1) MBSD of the Si wafer for comparison purposes and one can observe that $W\phi \gg W\omega$, the condition for a quasi perfect crystal (in the dynamical approach). Fig. 7 exhibits the mappings of the F_2 as-implanted ((a) and RTA-30 s (b)). We see an intensity asymmetry in omega corresponding to the tensile strain in the as-implanted sample, which confirms the rocking curve result. This asymmetry practically disappears for the MBSD of the annealed sample shown in Fig. 7(b). On the other hand, there is a stronger primary intensity (background) due to the presence of the ions in the Si lattice.

4. Conclusions

In this work, we have successfully applied BSD analysis of XRMD to study the shallow junctions of B in Si(0 0 1).

The diffusion of B in implanted Si(0 0 1) samples during annealing is enhanced by its interaction with interstitial Si. Therefore, the analysis of the interstitial rich region is crucial for the understanding of the shallow junction formation. The occurrence of a hybrid extra BSD peak, which represents the contribution from the interstitial rich region in the matrix RS, was used as a fine interface probe to investigate the behavior of this interstitial region as a function of the implantation energy and the thermal annealing condition.

The possibility of applying this structural characterization technique to other systems (such as single crystal model catalysts) is intriguing.

Acknowledgments

The authors would like to thank the LNLS staff for the measurements using synchrotron radiation at XRD1 station and G.G. Kleiman, for valuable discussions. The financial support from the Brazilian agencies FAPESP, CNPq and FINEP is also acknowledged.

References

[1] S.L. Morelhão, L.P. Cardoso, Solid State Commun. 88 (6) (1993) 465.
[2] S.L. Morelhão, L.H. Avanci, M.A. Hayashi, L.P. Cardoso, S.P. Collins, Appl. Phys. Lett. 73 (15) (1998) 2194.
[3] L.H. Avanci, L.P. Cardoso, S.E. Girdwood, D. Pugh, J.N. Sherwood, K.J. Roberts, Phys. Rev. Lett. 81 (24) (1998) 5426.
[4] L.H. Avanci, L.P. Cardoso, S.E. Girdwood, D. Pugh, K.J. Roberts, J.M. Sasaki, J.N. Sherwood, Phys. Rev. B 61 (10) (2000) 6507.
[5] L.H. Avanci, X. Lai, J.M. Sasaki, K.J. Roberts, L.P. Cardoso, J. Appl. Crystallogr. 36 (2003) 1230.
[6] M. Renninger, Z. Phys. 106 (1937) 141.
[7] S.L. Chang, Multiple diffraction of X-rays in crystals, Series in Solid-State Sciences, vol. 50, Springer-Verlag, Berlin, Heidelberg, New York, 1984.
[8] S.L. Morelhão, L.P. Cardoso, J. Appl. Cryst. 29 (1996) 446.
[9] S.L. Morelhão, L.P. Cardoso, J.M. Sasaki, M.M.G. de Carvalho, J. Appl. Phys. 70 (5) (1991) 2589.
[10] L.H. Avanci, M.A. Hayashi, L.P. Cardoso, S.L. Morelhão, F. Riesz, K. Rakennus, T. Hakkarainen, J. Cryst. Growth 188 (1998) 220.
[11] M.A. Hayashi, S.L. Morelhão, L.H. Avanci, L.P. Cardoso, J.M. Sasaki, L.C. Kretly, S.L. Chang, Appl. Phys. Lett. 71 (18) (1997) 2614.
[12] B.C. Larson, J.F. Barhorst, J. Appl. Phys. 51 (1980) 3181.
[13] S.L. Morelhão, J. Synchrotron Rad. 10 (3) (2003) 236.
[14] J. Klappe, I. Bársony, J.R. Liefiting, T.W. Ryan, Thin Solid Films 235 (1993) 189.